Meteorol Atmos Phys (2017) 129:539–554
DOI 10.1007/s00703-016-0484-7

ORIGINAL PAPER

Comparison of the diurnal variations of precipitation east of the Tibetan Plateau among sub-periods of Meiyu season

Yuanchun Zhang[1] · **Jianhua Sun**[1,2]

Received: 15 September 2014 / Accepted: 21 October 2016 / Published online: 1 November 2016

Abstract This study divides the Meiyu period (15 June–15 July) into three sub-periods according to the consecutive Meiyu precipitation days: TMY (typical Meiyu days; TMY), pre-TMY and post-TMY. It is shown that the eastward propagation and diurnal variations of precipitation during the three sub-periods are obviously different. The similar phase delay of precipitation from the eastern part of the Tibetan Plateau (TP) to the "second step" terrain during the three sub-periods is possibly caused by the propagation of precipitation systems originating from the eastern part of the TP, but the phase speed during the pre-TMY period is fastest due to the prevailing zonal wind speed. The precipitation continues to propagate eastward from the east of the "second step" terrain to the central Yangtze River valley during the pre-TMY and TMY periods, but the phase speed during the pre-TMY period is faster. During the post-TMY period, precipitation east of the "second step" terrain mainly appears in the afternoon. The diurnal variation of the horizontal wind anomaly and mountain–plain solenoid (MPS) circulations east of 110°E during the TMY period is more obvious than in the other two sub-periods. MPS circulations due to different terrain distributions are mainly responsible for forcing the diurnal cycles of precipitation over the TP and Sichuan Basin (SCB), but for the diurnal variation of precipitation over the Yangtze-Huai River Valley, MPS circulations coupled with the favorable synoptic patterns (Meiyu front) could intensify the precipitation and its diurnal cycles.

Responsible Editor: J. T. Fasullo.

✉ Yuanchun Zhang
zhyc@mail.iap.ac.cn

[1] Key Laboratory of Cloud-Precipitation Physics and Severe Storms (LACS), Institute of Atmospheric Physics, Chinese Academy of Sciences, P.O. Box 9804, Beijing 100029, China

[2] University of Chinese Academy of Sciences, Beijing 100049, China

1 Introduction

The diurnal cycles of precipitation frequency and intensity have marked effects on surface hydrology and could affect local weather and climate (Dai et al. 1999; Dai 2001). In recent decades, the diurnal variations in winds, convective activities, and precipitation during the warm season have been recognized as a key aspect affecting the geographic distribution of precipitation and development of convection (Wang et al. 2004; Hirose and Nakamura 2005; Yu et al. 2007; Chen et al. 2009a, b, 2012; Bao et al. 2011; Zhang et al. 2014a). Previous studies have shown that summertime convection in the US often develops over the Rocky Mountains in the local afternoon, and subsequently propagates eastward over the region east of the Rocky Mountains and its adjacent plains overnight due to the forcing from diurnally varying heating (Carbone et al. 2002; Carbone and Tuttle 2008; Trier et al. 2006, 2010). Recent studies have documented the diurnal variations of clouds and precipitation in East Asia using surface observations (e.g., Yu et al. 2007) and satellite observations (Geng and Yamada 2007; Chen et al. 2009a, b, 2012; Wang et al. 2004, 2005; Bao et al. 2011). Some studies have hypothesized the potential mechanisms influencing the diurnal cycles of precipitation, such as land–sea breezes, the downwind diabatic heating gradient, the diurnal variations of friction at boundary layers, low-level jets (LLJs), mountain–plain solenoid (MPS) circulations, and the propagation of convection from plateaus or mountain ranges (Blackadar 1957; Bonner 1968; Wallace

1975; Riley et al. 1987; Chen and Li 1995; Carbone et al. 2002; Zhang et al. 2002; Yasunari and Miwa 2006; He and Zhang 2010; Huang et al. 2010; Bao et al. 2011; Sun and Zhang 2012; Zhang et al. 2014a; Du et al. 2014).

The geographic distribution in the study area (shown in Fig. 1a) shows a three-step variation: the major terrain is the Tibetan Plateau (TP), which is often referred to as the "first step" terrain in China. The "second step" terrain usually refers to the high mountain ranges between the Qinling Mountains over central China and the Yunnan-Guizhou Plateau over southwest China. The "third step" terrain includes the low-lying plains and hilly regions to the east of the "second step" high-mountain terrains. The Meiyu front—a quasi-stationary, east–west-oriented frontal zone during summer along the Yangtze–Huai River Valleys (YHRV) (Tao 1980)—is one of the major heavy-rainfall-producing systems in East China (Zhao et al. 2004). Previous studies have provided insight into the diurnal variability of Meiyu, but most of them focused on the diurnal cycle during the whole summer/climatological Meiyu period, or cases of short periods. For example, recent studies divided the warm season into a pre-Meiyu period, Meiyu period, and post-Meiyu period and showed that the diurnal cycles of precipitation differ substantially from the eastern edge of the TP to the YHRV during the three periods (Bao et al. 2011; Xu and Zipser 2010). During the Meiyu period, the propagating systems from the east slope of the TP to the middle reach of YRV support the eastward migrating events. Morning rainfall arising from a local growth of rain events forms and develops in the areas with nocturnal southwesterlies of warm/moist air impinging on the Meiyu front in the lower troposphere (Chen et al. 2013). Other studies also show that the eastward propagation of a rainfall streak from the

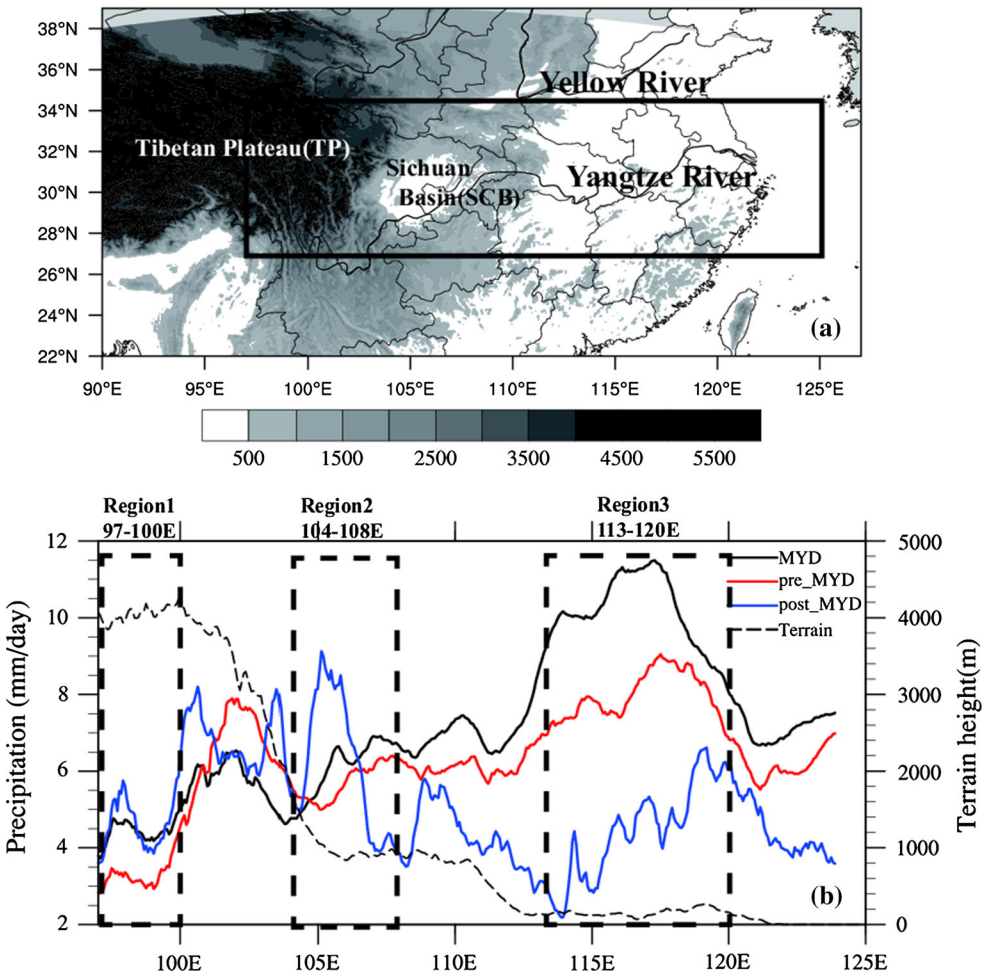

Fig. 1 **a** Terrain distribution over East China (*shading*, units: m). The *black box* indicates the study domain (27°–35°N, 100°–125°E). **b** Daily precipitation averaged over 27°–35°N during the TMY (*black line*), pre-TMY (*red line*), and post-TMY (*blue line*) periods. The longitudinal terrain height (*black dashed lines*) is averaged over the areas in the *black box* in **a**, and the division of the three regions is shown (*black dashed boxes*)

eastern edge of the TP to the eastern coastal region is primarily due to a series of convective activities of several systems from west to east, including the MPS between the TP and Sichuan Basin (SCB), southwest vortices (mesoscale vortex over Southwest China at 700 or 850 hPa forced by the terrain effect of TP, Tao 1980), and the MPS between the "second step" terrain and the east plains (Zhang et al. 2014b). Additionally, Chen et al. (2013) showed that diurnal variation of low-level wind is pronounced over South China on active monsoon days. They illustrated that nocturnal moisture fluxes converge toward central China and lead to a meso-synoptic-scale moisture sink during the late night and morning, which plays a role in regulating the regional water budget on a diurnal timescale.

The focus area of the study is from the eastern part of TP to the YHRV of the East China plains during the Meiyu season. According to the annual Meiyu period recorded by the National Climate Center (NCC), Chinese Meteorology Administration (CMA), actual Meiyu days (consecutive rainy days) are much shorter than the Meiyu period defined by Bao et al. (2011) and Xu and Zipser (2010) (Tables 1, 2); diurnal cycles of precipitation during actual Meiyu days could be different with the former defined Meiyu period. It is necessary to show and compare the diurnal cycles and eastward propagation of precipitation during the three sub-periods of the climatological Meiyu period (CMYP; 15 June–15 July), which could be favorable to understand the mechanisms of eastward propagation of precipitation during actual Meiyu days. There are several sections in the following text. Section 2 of the paper introduces the data and method used in this work. Section 3 describes the diurnal variations of precipitation during the three sub-periods of the CMYP. Section 4 analyzes the potential mechanisms affecting the diurnal cycles. Finally, a summary and discussion are presented in Sect. 5.

2 Data and methodology

The primary dataset used in this work is the high temporal and spatial resolution global precipitation dataset from the National Oceanic and Atmospheric Administration (NOAA) Climate Prediction Center (CPC) morphing technique (CMOPRH; Joyce et al. 2004). The dataset covers 60°S to 60°N with a spatial resolution of 0.07277° and temporal resolution of 30 min. Previous studies have evaluated the performance of CMORPH data compared with gauge-based analysis of hourly precipitation and other satellite precipitation (Shen et al. 2010; Luo et al. 2013). Their comparisons show that the satellite products tend to underestimate the morning peak of the Meiyu rainfall over central China. However, the CMORPH precipitation could be capable of detecting the spatial pattern and temporal variation in East China, the overall features of the diurnal variations and the eastward phase propagation of the heavy precipitation along the Meiyu frontal system (Shen et al. 2010; Luo et al. 2013). In addition, the National Centers for Environmental Prediction (NCEP) Global Forecast System (GFS) Final (FNL) (1° × 1°) dataset with a temporal resolution of 6 h is used for analyzing circulations related to the diurnal variation, and the six-hourly climate forecast system reanalysis (CFSR) data (0.5° × 0.5°) from the National Centers for Environment Prediction (NCEP) with higher vertical resolution is used to describe the MPS circulations. To further analyze the different characteristics of the diurnal cycles during different periods of climatological Meiyu days, in the present study, we divide the climatological Meiyu period (CMYP; 15 June–15 July, 2003–2010) into typical Meiyu days (TMY, consecutive rainy days, shown in Table 1) and non-typical-Meiyu days (NTMY). Typical Meiyu days are the annual Meiyu period published by the NCC/CMA, and to obtain a better comparison of the diurnal variations and eastward propagation of precipitation systems during different periods, the non-

Table 1 Periods of climatological Meiyu, typical Meiyu days, and non-typical-Meiyu days from 2003 to 2010

Year	Climatological Meiyu period (CMYP) (217 days)	Typical-Meiyu days (TMY) (103 days)	Non-typical Meiyu days (125 days)	
			Pre-typical-Meiyu days (pre-TMY) (73 days)	Post-typical Meiyu days (post-TMY) (52 days)
2003	June 15–July 15	June 21–June 29; July 5–July 11	June 15–June 20; June 30–July 4	July 12–July15
2004		June 14–June 25	N/A	June 26–July 15
2005		July 5–July 14	June 15–July 4	July 15
2006		July 5–July 11	June 15–July 4	July 12–July 15
2007		June 19–July 14	June 15–June 18	July 15
2008		June 7–June 23	N/A	June 24–July 15
2009		N/A	N/A	N/A
2010		July 3–July 17	June 15–July 2	N/A

Table 2 Comparison of previous studies and present study

	Motivation of period definition	Period definition	Propagation of precipitation during different periods	Mechanism of nocturnal precipitation maximum over eastern plain
Xu and Zipser (2010)	Onset of monsoon	Pre-Meiyu (1 April–11 May); Meiyu (15 May–25 June); Mid-summer (1 July–10 August)	Evident precipitation propagation from eastern TP to SCB during pre-Meiyu and Meiyu season	Long-lived MCSs evolving from late afternoon or early night convection
Bao et al. (2011)	Climatological mean position of the primary rainband during warm season	Pre-Meiyu (15 May–15 June); Meiyu (15 June–15 July) Post-Meiyu (15 July–15 August)	Eastern TP to coastal plain (120°E) Eastern TP to eastern slope of the "second step" terrain (110°E) Eastern TP to west of 113°E	Upward branch of a mountain–plain solenoid (MPS) and nocturnal low-level jet (LLJ)
Present study	Actual consecutive rainy days during Meiyu season (shown in Table 1)	Pre-typical Meiyu days (pre-TMY) (shown in Table 1) Typical Meiyu days (TMY) (shown in Table 1) Post-typical-Meiyu days(post-TMY); (shown in Table 1)	Eastern TP to eastern plains (115°E) Eastern TP to eastern slope of the "second step" terrain (110°E) Continuation of propagation over YHRV along Meiyu front Eastern TP to eastern slope of the "second step" terrain (110°E)	In the western part of the Meiyu front: Nocturnal LLJ, convergence belt and the upward branch of MPS (S2) In the eastern part of the Meiyu front: MCV and moist convection combining with the upward branch of MPS (S3)

typical-Meiyu days are divided into pre-TMY and post-TMY (shown in Table 1). Pre-TMY is the time period before TMY during the CMYP and post-TMY is the time period after TMY during the CMYP. Due to the non-Meiyu event of summer 2009, we exclude dataset from that year. The years of 2004 and 2008 are not in the average of pre-TMY and the year of 2010 is not in the average of post-TMY (Table 1). The domain focused upon in this study is (27°–35°N, 97°–125°E) (Fig. 1a), including the eastern TP, Sichuan Basin (SCB) and YHRV. The terrain height shows an obvious three-step distribution: the "first step" is the eastern part of the TP; the "second step" terrain includes the SCB and adjacent mountain ranges; the "third step" covers the YHRV in eastern China. Three sub-regions of the study domain (areas covered by black boxes in Fig. 1a) are selected for analysis (Fig. 1b) to better compare the diurnal variations of precipitation over these different terrains: eastern part of the TP (97°–100°E, Region 1); SCB region (104°–108°E, Region 2); eastern plains (113°–120°E, Region 3).

The standard deviation of hourly precipitation symbolizes the intensity of diurnal variation, and the formula to calculate standardization is $x(t) = (X(t) - \bar{X})/\sigma$, where σ is the standard deviation, $\sigma = \sqrt{\frac{1}{N}\sum_{t=1}^{N}(X(t) - \bar{X})^2}$, and N is the number of samples (Wilks 2006).

3 Diurnal variation and eastward propagation of precipitation systems east of the TP during different periods

3.1 CMYP

Figure 2a shows the Hovmöller diagram of standardized precipitation during the CMYP averaged from 2003 to 2010 in our study domain (time is Beijing standard time, BST = UTC + 8). During the CMYP, the precipitation maximum at the eastern part of the TP appears in the afternoon to the late night (1400–0300 BST), arrives in the SCB in the midnight to early morning (0000–0900 BST), and propagates eastward at the eastern edge of the "second step" terrain (~110°E) in the afternoon to early evening (1200–1800 BST). Over the East China Sea (east of 122°E), compared with its adjacent land areas, the diurnal variation of precipitation shows the opposite phase, with the maximum appearing in the late night to noon (0300–1200 BST). The diurnal variations of precipitation east of the "second step" terrain, which is the location of the typical Meiyu rain belt, are quasi-stationary with the peak in the noon to early evening (1200–1800 BST). However, a previous study demonstrated that the precipitation maximum over the YHRV during the Meiyu period appears in the early morning (Geng and Yamada 2007).

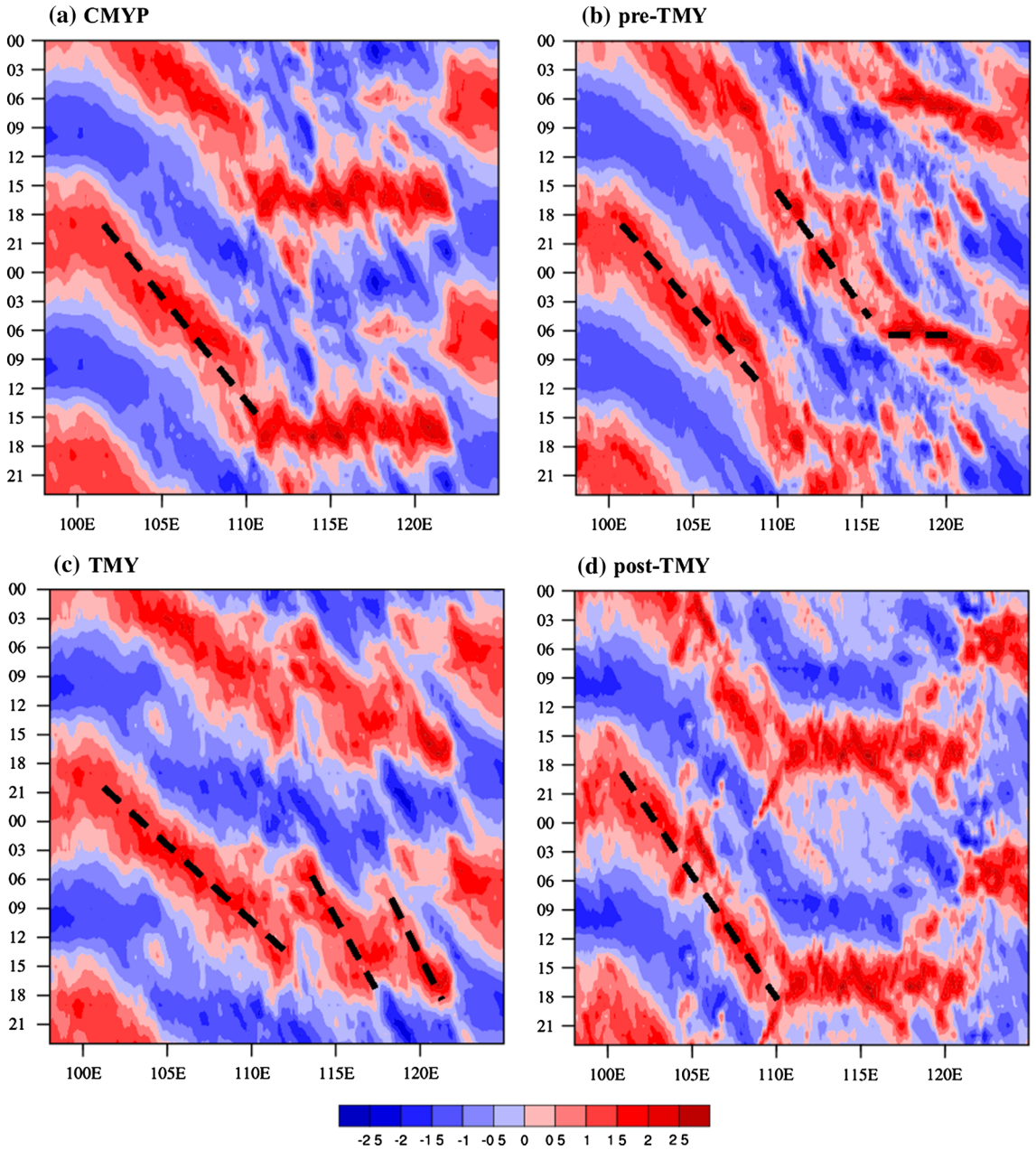

Fig. 2 Time–longitudinal sections of normalized precipitation anomalies averaged between 27°N and 35°N during the **a** CMYP, **b** pre-TMY period, **c** TMY period, and **d** post-TMY period. Time is BST. *BST* Beijing standard time

The precipitation of typical Meiyu cases in 2007 peaked in the late evening to early morning (Sun and Zhang 2012). According to the information shown in Table 1, consecutive rainy days (actual Meiyu days) are fewer in number than non-rainy days (non-Meiyu days) during the CMYP from 2003 to 2010. It is possible that the phases of diurnal variation of precipitation during TMY (actual Meiyu days) and non-typical Meiyu days are different. In the following sections, we compare and discuss the diurnal variations of precipitation among the TMY, pre-TMY and post-TMY periods.

3.2 Pre-TMY period

The daily precipitation of the pre-TMY period is about 5–9 mm day^{-1} from the east part of TP to the coastal area (Fig. 1b), and has a maximum in the east plains (116°E–118°E) and a minimum in the SCB. It has the smallest variation among the different sub-periods of the CMYP. During the pre-TMY period (Figs. 2b, 3), similar to that during the CMYP, the precipitation maximum over the eastern part of the TP appears in the afternoon to late night (1500–0200 BST), arrives at the SCB (~105°E) in the late

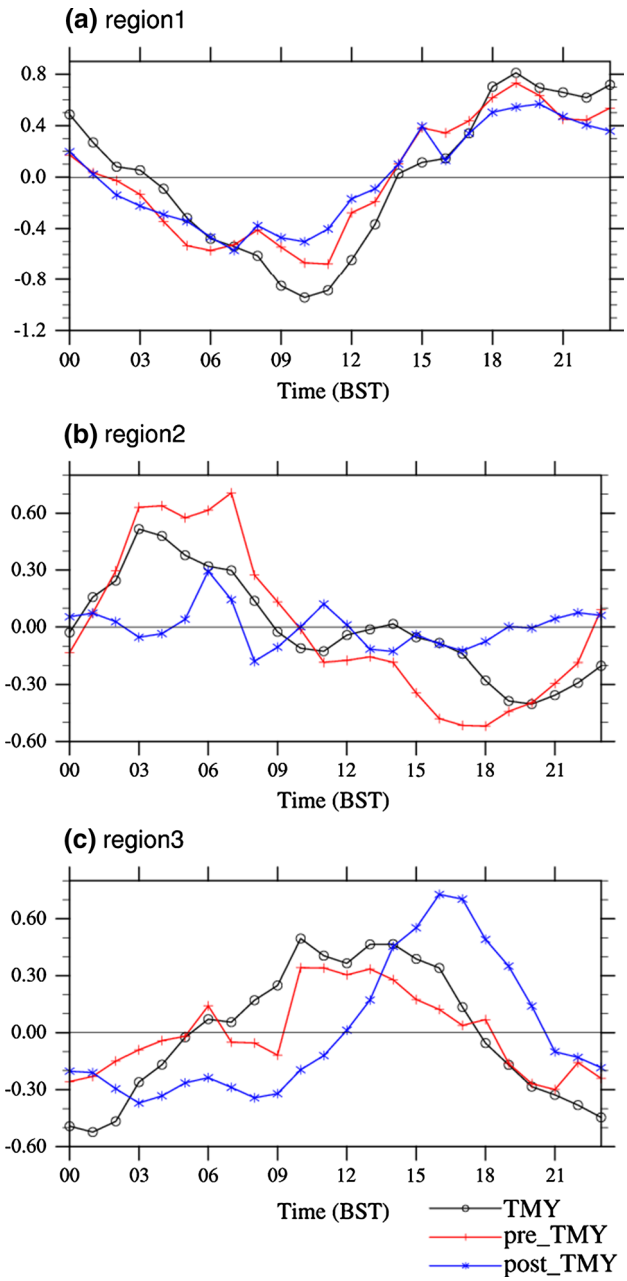

Fig. 3 Diurnal variation of standardized precipitation over the three regions shown in Fig. 1b during the pre-TMY (*red lines* with *crosses*), TMY (*black lines* with *circles*), and post-TMY (*blue line* with *asterisks*) periods

night to early morning (0100–0900 BST), and propagates eastward over the east of the "second step" terrain (~110°E) in the afternoon (~1200 BST) at a phase speed of ~17.8 m s^{-1}. After that, the diurnal variations east of the SCB during the pre-TMY period are different from those during the CMYP. The precipitation maximum over the middle reaches of the YHRV east of 110°E appears after 1500 BST and continues to propagate eastward to 115°E at a phase speed of 14.3 m s^{-1}, which is consistent with the phase speed of ~10–25 m s^{-1} in the study by Wang et al. (2004, 2005) and the main phase speed derived from the wavenumber–frequency power spectrum of hourly precipitation by Zhang et al. (2014a) over East Asia. The quasi-stationary rainfall peak over the YHRV appears at 1500–0000 BST in the western YHRV (113°–116°E) and at 0300–0700 BST in the eastern YHRV (116°–120°E), and strong precipitation over the East China Sea appears in the late night to early morning—the opposite phase to that over land areas.

From west to east, the average daily precipitation east of the TP shows varying intensity, which is possibly, affected by the distribution of terrain and general circulations. We document the details and differences of the diurnal variations among the three regions (Fig. 1b) in Fig. 3. In the eastern part of the TP (Region 1, R1), strong precipitation occurs in the afternoon to the late night (1500–0200 BST) with a maximum at 1900 BST, and weak precipitation appears in the late night to the afternoon (0300–1400 BST). In the SCB (Region 2, R2), nocturnally strong precipitation occurs during 0100–0900 BST with two peaks appearing at 0300 and 0700 BST. Over the east plains (R3), the average diurnal variations cannot represent the characteristics in Fig. 2b, possibly because of the different local circulations and diurnal variations between the middle and lower reaches of the YHRV. The above analysis demonstrates that the duration of strong precipitation from the eastern part of the TP (R1) to the east plains (R3) shows obvious consecutive phase delay, which is consistent with the precipitation propagation shown in Fig. 2b.

3.3 TMY period

The daily precipitation of the pre-TMY period has the smallest variation among the different sub-periods of the CMYP, which is ~5 mm day^{-1} over the SCB and increases to ~9 mm day^{-1} over the east plains (Fig. 1b). The average daily precipitation during the TMY period is lower than that during the pre-TMY period west of 105°E, but east of 108°E it is the highest among the three sub-periods. It is possible that the maintenance of the Meiyu front enhances the precipitation east of the "second step" terrain. The diurnal variation over the TP and SCB during the TMY period is almost the same as that during the pre-TMY period. The eastward propagation of precipitation systems from the eastern part of the TP arrives at the eastern slope of the "second step" terrain in the afternoon (~1500 BST), but the phase speed (15.2 m s^{-1}) is a little slower than that during the pre-TMY period (Fig. 2b, c). The precipitation east of the "second step" terrain (113–115°E) begins to strengthen in the late night (at ~0300 BST); then, combined with convection originating from the TP, propagates at 113°E, and continues to

propagate eastward to the YHRV during 1200–1800 BST at a speed of 10.2 m s^{-1}. Additionally, the continuation of the precipitation propagation over the YHRV (117°–121°E) is possibly forced by the movement of convection along the Meiyu rainbelt. The diurnal variations of precipitation during the TMY period over the eastern coastline also show an early-morning precipitation maximum.

The diurnal variations of normalized precipitation are similar to that during the pre-TMY period over the eastern part of the TP (R1) (Fig. 3a), and high precipitation also appears in the afternoon to late night (1400–0200 BST) with the peak at 1800 BST. Over the SCB (R2), nocturnal precipitation occurs in the late night to the following morning (0100–0800 BST) with the maximum at 0300 BST. Over the Yangtze-Huai River Valley (YHRV, R3), high precipitation appears during 0600–1700 BST with peaks at 1000 BST and 1400 BST. The precipitation maximum appears in the early morning and afternoon, which is different with the early-morning precipitation peak (Geng and Yamada 2007). The possible reason is that only the Meiyu periods in 2003 and 2007 are typical during 2003–2010 (Sun et al. 2006; Sun and Zhang 2012). The average of 2003–2010 cannot show the typical nocturnal precipitation over Meiyu front along Yangtze-Huai River Valley (Geng and Yamada 2007; Sun and Zhang 2012). During TMY in 2007, the diurnal variation of precipitation shows two precipitation peaks in 24 h and obvious early-morning peak, but strong precipitation appears in daytime during TMY in 2006 with peak in the morning (not shown). In Fig. 2c, it is clear that the diurnal characteristics in the western and eastern parts along Yangtze River east of the "second step" terrain are different. Only the precipitation in the western part has the early-morning precipitation peak. As discussed by Sun and Zhang (2012), moist convection initiated in the western part of the Meiyu front with an early-morning precipitation peak subsequently leads to the formation of mesoscale convective vortices (MCV). Then the MCV amplifies moist convection in the eastern part of the Meiyu front while propagating eastward along it. The average cannot show the typical diurnal variation of the Meiyu rain belt over different regions, which demonstrates the complexity of diurnal variation.

3.4 Post-TMY period

The distribution of average daily precipitation during the post-TMY is different to that during the former two sub-periods (Fig. 1b). The daily precipitation west of 110°E is higher than that in the YHRV, and the maximum appears over the SCB. During the post-TMY period, the major rain belt is located over the YHRV (Fig. 4c). The diurnal variations and eastward propagation of the precipitation anomaly from the eastern part of the TP (~100°E) to the "second step" terrain (~110°E) are basically consistent with that during the CMYP (Fig. 2d). The phase speed (~10.4 m s^{-1}) is slower than that during the TMY period. From the middle of the YHRV to the coastal area (east of the "second step" terrain), high precipitation appears during 1300–2000 BST without propagation.

The diurnal variation of precipitation over the different regions during the post-TMY period (Fig. 3) shows that the diurnal variation over the eastern part of the TP is almost consistent with the former two periods. Over the SCB, precipitation mainly appears in the early evening to the following morning (1800–0700 BST) with the peak at 0600 BST, which is similar to the precipitation peak of pre-TMY appearing in the early morning, but 3 h later than that in TMY. However, east of the SCB, the diurnal variation of precipitation is obviously different to that during the former two periods. The obviously high precipitation appears during 1300–2000 BST with the peak at 1600–1700 BST over the YHRV.

The above analysis shows that the average daily precipitation and diurnal variations of precipitation over the eastern part of the TP and its eastern slope during the three sub-periods are consistent with each other. Additionally, a phase delay of strong precipitation exists from the eastern part of the TP to the SCB during the three sub-periods, which is possibly caused by the propagation of precipitation systems originating from the eastern part of the TP (Wang et al. 2004, 2005; Chen et al. 2013). But east of the SCB, the diurnal variations of precipitation during the pre-TMY and TMY periods are much more similar and also show a consecutive phase delay; however, during the post-TMY period, high precipitation mainly appears in the afternoon east of the "second step" terrain. The precipitation has an early-morning peak in the western part of the Meiyu rain belt and afternoon peak in the eastern part.

4 Mechanisms of precipitation diurnal variation during the three sub-periods

As described above, due to the maintenance of the Meiyu front, the CMYP is divided into the TMY, pre-TMY and post-TMY sub-periods, and the eastward movement of precipitation systems and their diurnal variation are determined/affected by the background circulations during these three sub-periods as well as the local circulation forced by the distribution of terrain. In this section, the background circulations and MPSs between the TP ("second step" terrain) and the SCB (east plains) are compared and analyzed.

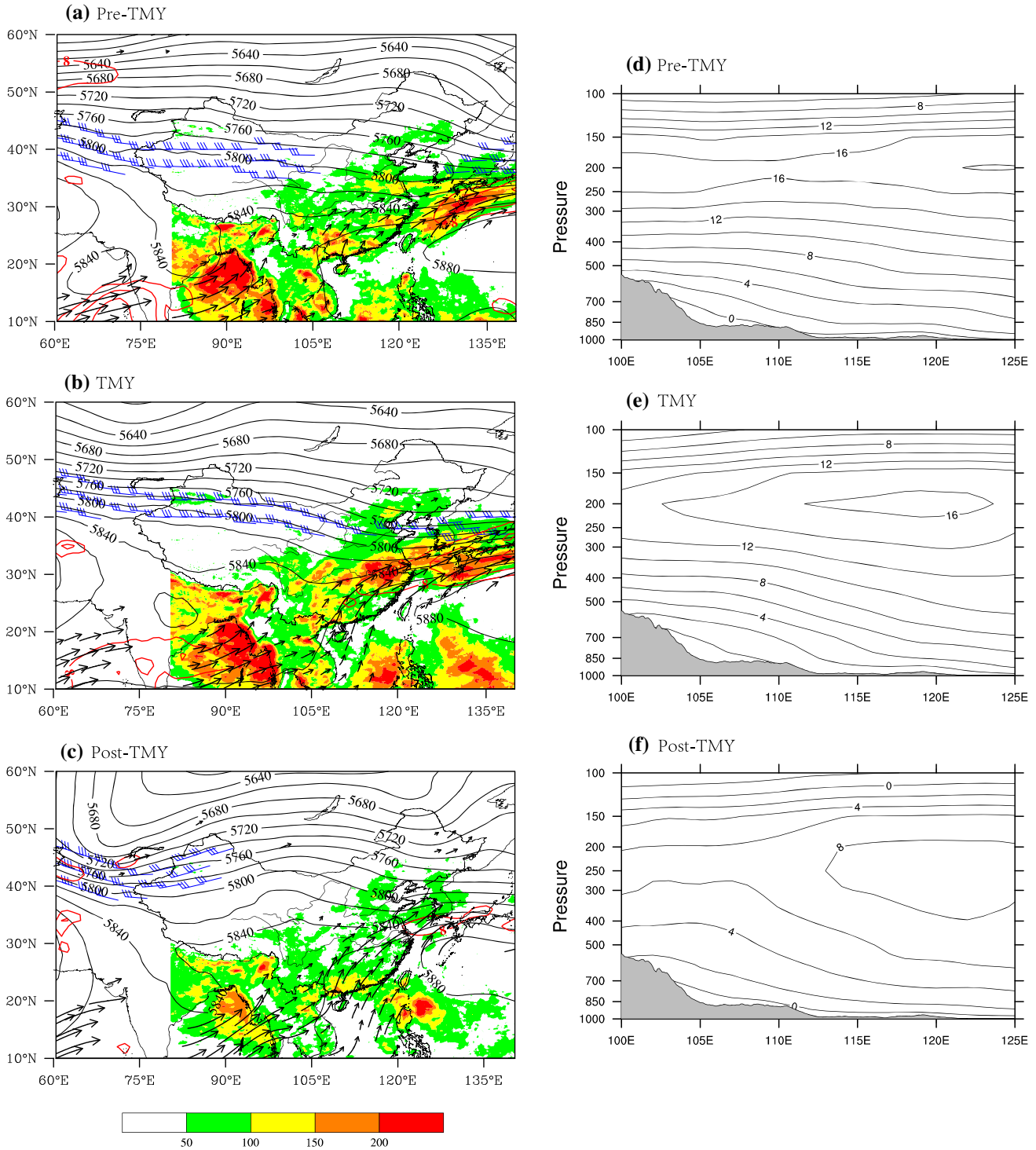

Fig. 4 Background circulation (geopotential height at 500 hPa, *black lines*; wind speed ≥30 m s^{-1} at 200 hPa, *blue* wind barbs; wind speed ≥8 m s^{-1} at 850 hPa, *red lines*) water vapor flux of the total levels (integrated from surface to 100 hPa, vector, units: kg m^{-1} s^{-1}) and averaged total precipitation (*shading*, mm) during the **a** pre-TMY, **b** TMY, and **c** post-TMY periods. Longitude–pressure cross sections of averaged zonal wind speed over 27°–35°N during the **d** pre-TMY, **e** TMY, and **f** post-TMY periods. The *gray shading* symbolizes the terrain distribution

4.1 Differences of average background circulations

During the pre-TMY period (Fig. 4a), the rain belt is located over South China, the YHRV, and oceanic areas north of the Western Pacific Subtropical High (WPSH). The rain belt over the YHRV is weaker than that over South China. At 200 hPa, there are two parts of the mid-latitude wind speed maxima at upper levels (over 40°–45°N): a western part that extends at approximately 105°E, and an eastern part located east of 125°E. At 500 hPa, the westerlies cover the mid and high latitudes and the WPSH controls the areas south of 30°N, with the 5860-gpm isohypse reaching as far as 105°E. The wind speed maxima at 850 hPa mainly controls the areas north of the WPSH and south of the Japanese archipelago, consistent with the location of the strongest rain belt. During the TMY period (Fig. 4b), the rain belt extends from the foothills of the Tibetan Plateau to the East China plains with an average maximum accumulated precipitation of more than 200 mm. The WPSH at 500 hPa dominates over southeastern China, with the 5860-gpm isohypse reaching as far west as 105°E and as far north as 28°N. In the mid-latitudes, there are two low troughs located at Lake Baikal and over northeast China, while a

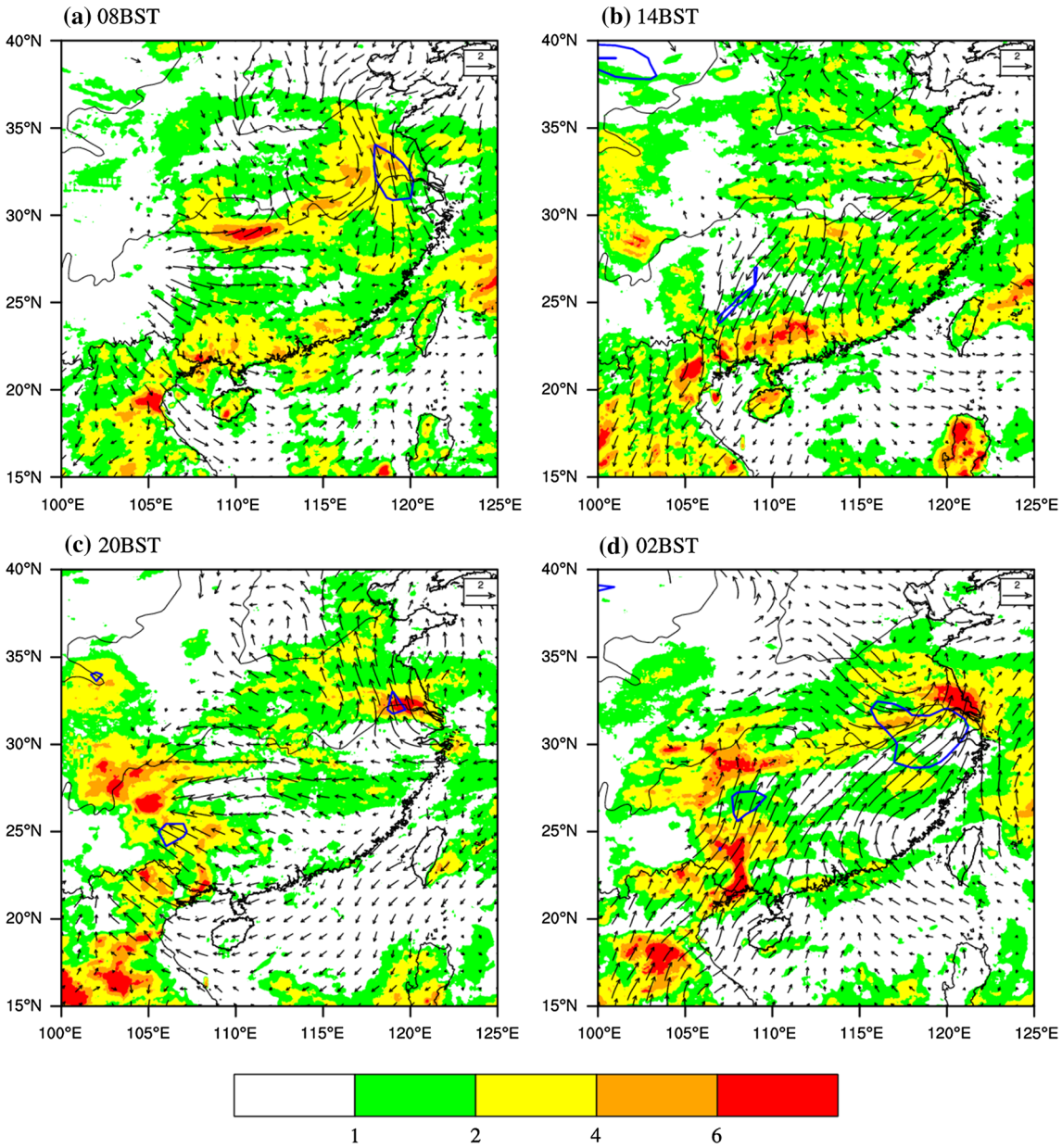

Fig. 5 Diurnal variation of horizontal wind perturbation at 850 hPa (vectors, m s^{-1}), 6-h accumulated precipitation (*shading*, mm), and wind anomaly speed (*blue lines*) during the pre-TMY period

weak ridge system controls northwest China. A weak trough east of the TP is conducive to convergence and moisture transportation over the YHRV. At 200 hPa, the midlatitude jet stream persists north of 40°N. Compared with the intensity of the wind speed maxima at lower levels (850 hPa) during the pre-TMY period, the wind speed south of the rain belt that is obviously intensified with stronger water vapor flux from South China Sea and the Bay of Bengal covers South China and Yangtze River Valley. During the post-TMY period (Fig. 4c), the wind speed maxima at 200 hPa retreats west of 90°E. A weak ridge covers from west China to the YHRV at 500 hPa, and the wind speed maxima at lower levels retreats over the Yellow Sea and weaker water vapor flux corresponds with the weaker precipitation compared to the former two periods. The above analysis shows that the background configurations are varied during the three sub-periods from 15 June to 15 July. The wind speed maxima at upper levels over central and eastern areas of China and the trough at 500 hPa possibly favor the eastward propagation of convection from eastern areas of the TP (Bao et al. 2011). Meanwhile, during the TMY period, the northern area of the WPSH with the wind speed maxima at lower levels (average wind speed at

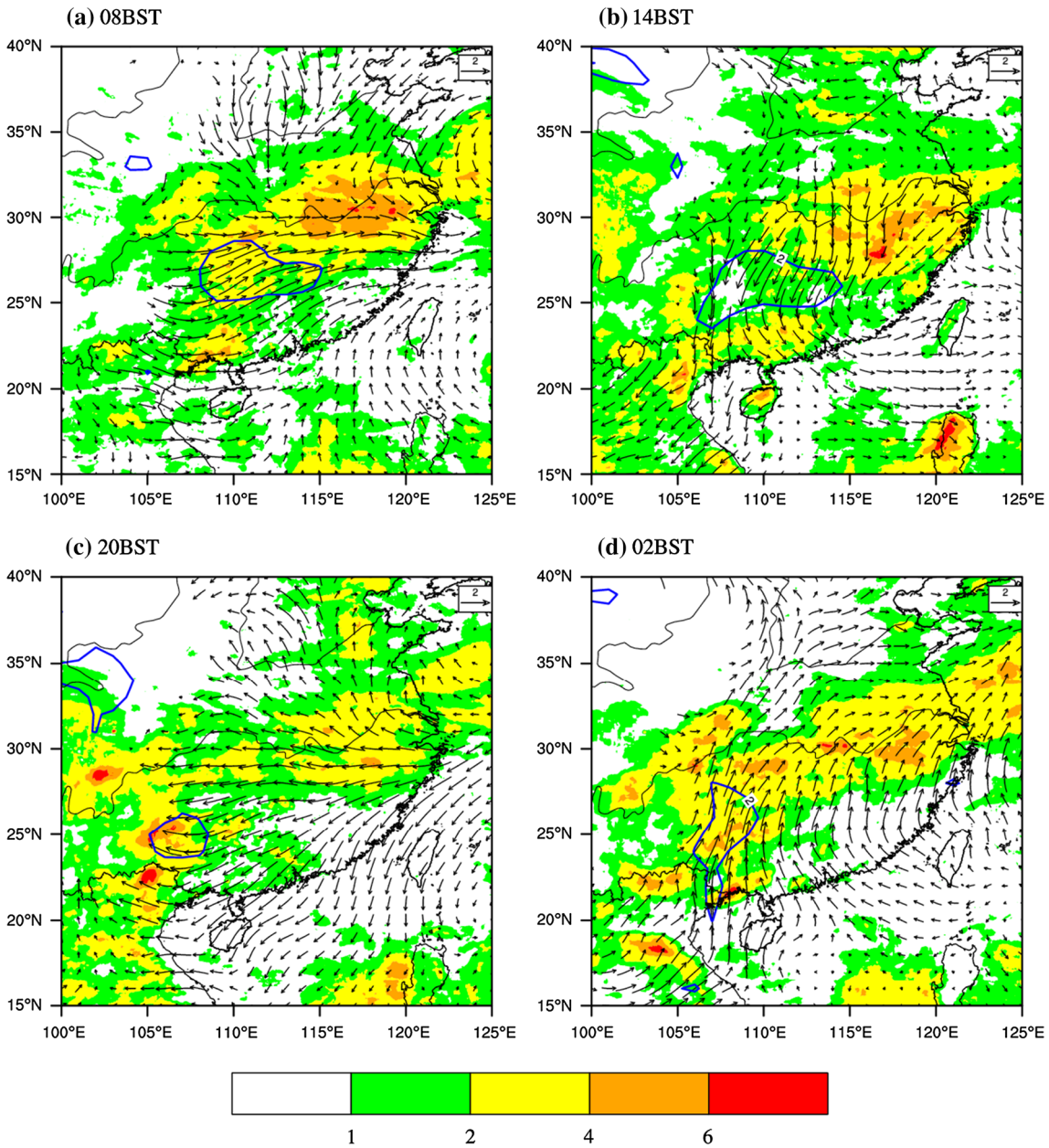

Fig. 6 The same as Fig. 5, but for the TMY period

850 hPa > 8 m s^{-1}) transports abundant water vapor. The above favorable ambient fields cause the strong precipitation over the YHRV.

The propagation speed of precipitation systems is associated with steering wind (Bao et al. 2011), the longitude–pressure cross sections of zonal wind averaged over 27°–35°N are shown in Fig. 4d–f. The zonal wind speed from the eastern part of the TP to the "second step" terrain at the middle and upper levels (100°–110°E) during the pre-TMY period is fastest among the three sub-periods, consistent with the fastest eastward propagation during the pre-TMY period (Fig. 2b–d). From the "second step" terrain to the middle reaches of the YHRV (110°–115°E), the zonal wind speed during the pre-TMY period is also the fastest, which is consistent with the eastward propagation of precipitation systems, as shown in Fig. 2b. From the pre-TMY to the post-TMY period, the westerly winds decrease significantly, especially in the post-TMY period, in which the wind speed is only half of that in the pre-TMY and TMY periods. The zonal wind influences the eastward propagation of convection from the eastern part of the TP to the YHRV.

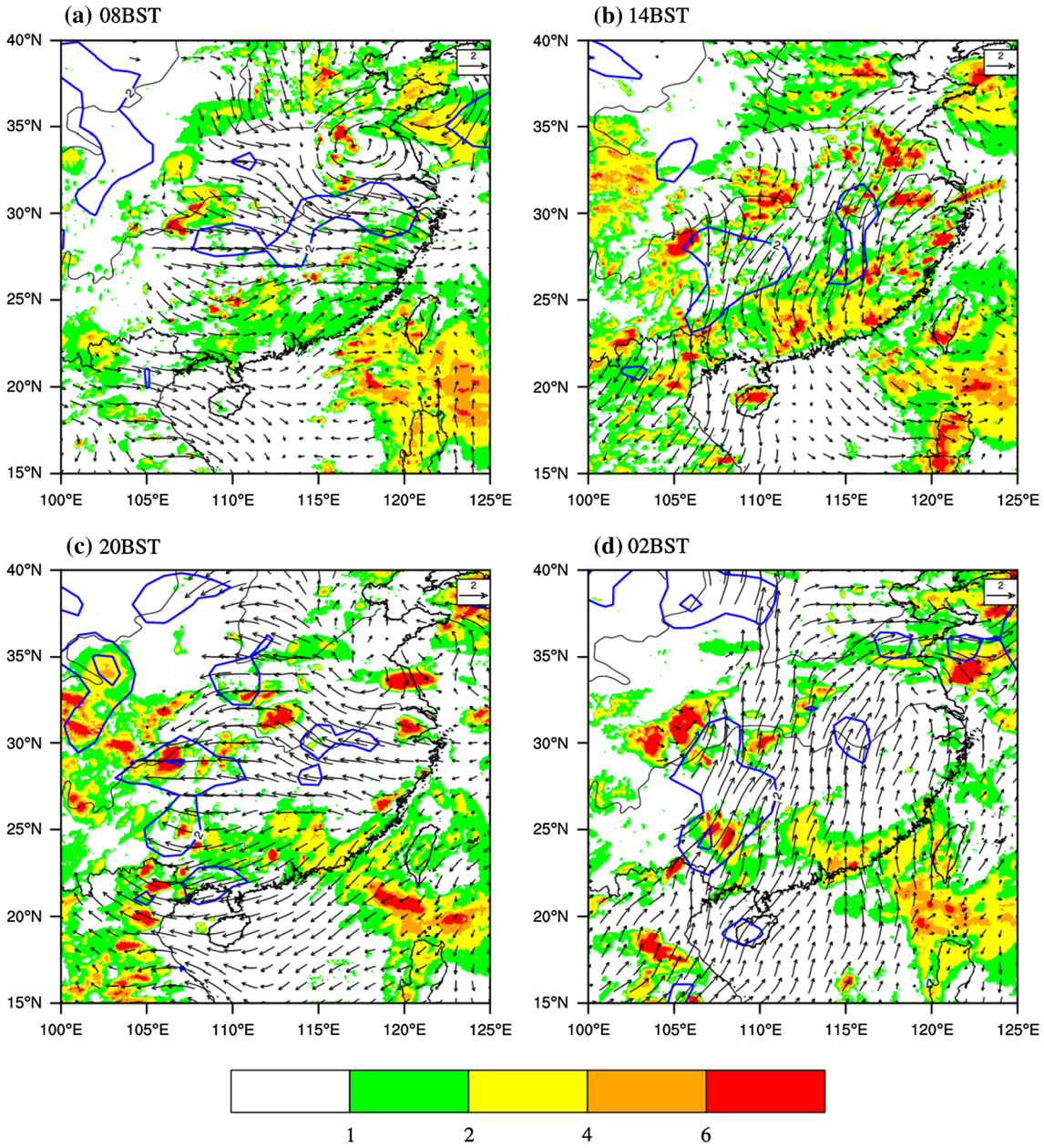

Fig. 7 The same as Fig. 5, but for the post-TMY period

4.2 Diurnal variations of MPSs and the wind field during the three sub-periods

The background circulation analysis only explains the variations of the rain belt's location and intensity and its eastward propagation during the three sub-periods. In this section, we document the diurnal variations of background systems and local circulations related to the distribution of terrain to understand the differences in diurnal variations among the three sub-periods.

Figures 5, 6 and 7 show the diurnal variations of the horizontal wind anomaly at 850 hPa and the 6-h accumulated precipitation during the three sub-periods. During the pre-TMY period (Fig. 5), the diurnal variations of the wind anomaly over northern and southern areas of 30°N are different. From the morning (0800 BST) to late night (0200 BST), the direction of the wind anomaly rotates clockwise over southern China (south of 30°N). In the daytime, the northern wind anomaly at 1400 BST shifts to an easterly wind anomaly at 2000 BST. During nighttime, the easterly wind anomaly rotates to become a southwesterly wind anomaly at 0200 BST. The diurnal variations of wind speed are 2–3.5 m s^{-1} at the lower level (850 hPa). The northwesterly wind anomaly at 0200 BST north of the Yangtze River valley converges with the southwesterly wind anomaly south of the Yangtze River valley. The convergence belt favors the enhancement of precipitation in the late night to early morning (Fig. 2b).

Similar to the pre-TMY period, the horizontal wind anomaly also shows clockwise rotation from day to night during the TMY period (Fig. 6). At 0200 BST, the southwesterlies anomaly extends northward to the YHRV (35°N) during the TMY period, and the abundant water vapor transported by the strong wind anomaly over East China intensifies the precipitation. At 0800 BST, the westerlies anomaly extends from the TP to the coastal area. The strong convergence between the northeasterly and southwesterly wind anomalies induces strong rain belt remaining over the YHRV. However, during the pre-TMY period, the southwesterlies anomaly in the pre-TMY period only controls the regions south to Yangtze River and the westerlies anomaly at 0800 BST only covers the

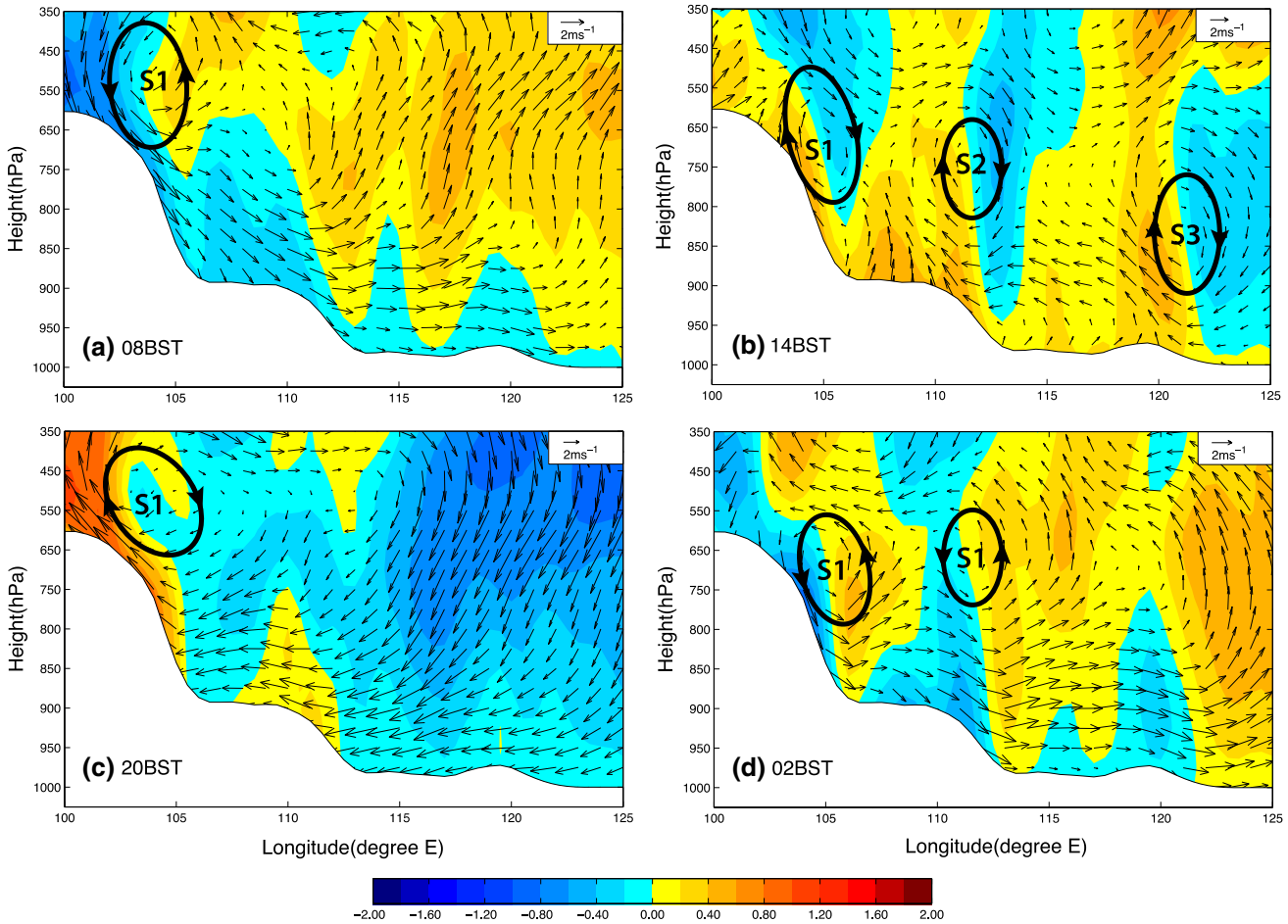

Fig. 8 Diurnal variation of the perturbation of vertical velocity (*shading*, cm s^{-1}) and vectors of anomalous zonal winds and anomalous vertical velocity (×100) during the pre-TMY period. S1, S2 and S3 represent three MPS circulations

area west of 115°E with weaker convergence over the YHRV.

Over East China during the post-TMY period (Fig. 7), northeasterly wind shifts to become easterly wind during the daytime (1400–2000 BST), and during the late night to early morning (0200–0800 BST) the direction of the wind anomaly rotates to become a southerly wind anomaly, further extending to the Yellow River regions. At 0800 BST, the directions of the wind anomaly over southern and northern areas of the Yangtze River valley are different, and the YHRV is covered by a westerly to northwesterly wind anomaly. The 6-h accumulated precipitation during the post-TMY period over the YHRV is lowest, but with relatively strong precipitation in the afternoon (1400 BST).

The comparison of the diurnal variations of the low-level horizontal wind anomaly and precipitation during the three sub-periods illustrates that the strongest southwesterlies appear in the late night to early morning. Additionally, southwesterly wind gradually extends northward from south of the Yangtze River valley to the Yellow River from the pre-TMY to the post-TMY period. The diurnal variations of the wind anomaly are consistent with the results of Chen et al. (2013). The peak of water vapor transported by the strong southwesterly wind occurs in the late night to early morning. However, the diurnal variations of precipitation during the three sub-periods are different, and do not agree well with that of the wind anomaly.

Previous studies have illustrated that MPS circulation is one of the key factors influencing the diurnal characteristics of Meiyu front precipitation. The coupling between MPS and large-scale circulation could explain the enhanced morning rainfall (Bao et al. 2011; Sun and Zhang 2012). Due to diabatic heating difference between obvious topographic contrasts, there are three daytime circulations (S1, S2, S3) with the upward perturbation forming over the eastern part of the TP, the "second step" terrain and the eastern coastlines, and downward perturbation in daytime appearing over the basin areas, the east plains and the oceanic area (Figs. 8b, 9b, 10b). Because of the wide descending branches of S2 in the afternoon during TMY, the suppressed southwesterlies (northeasterly anomaly in Fig. 6b) do not favor water vapor transportation, which cause the weak daytime precipitation at the western Meiyu rain belt (Fig. 9b). Only one obvious circulation appears at

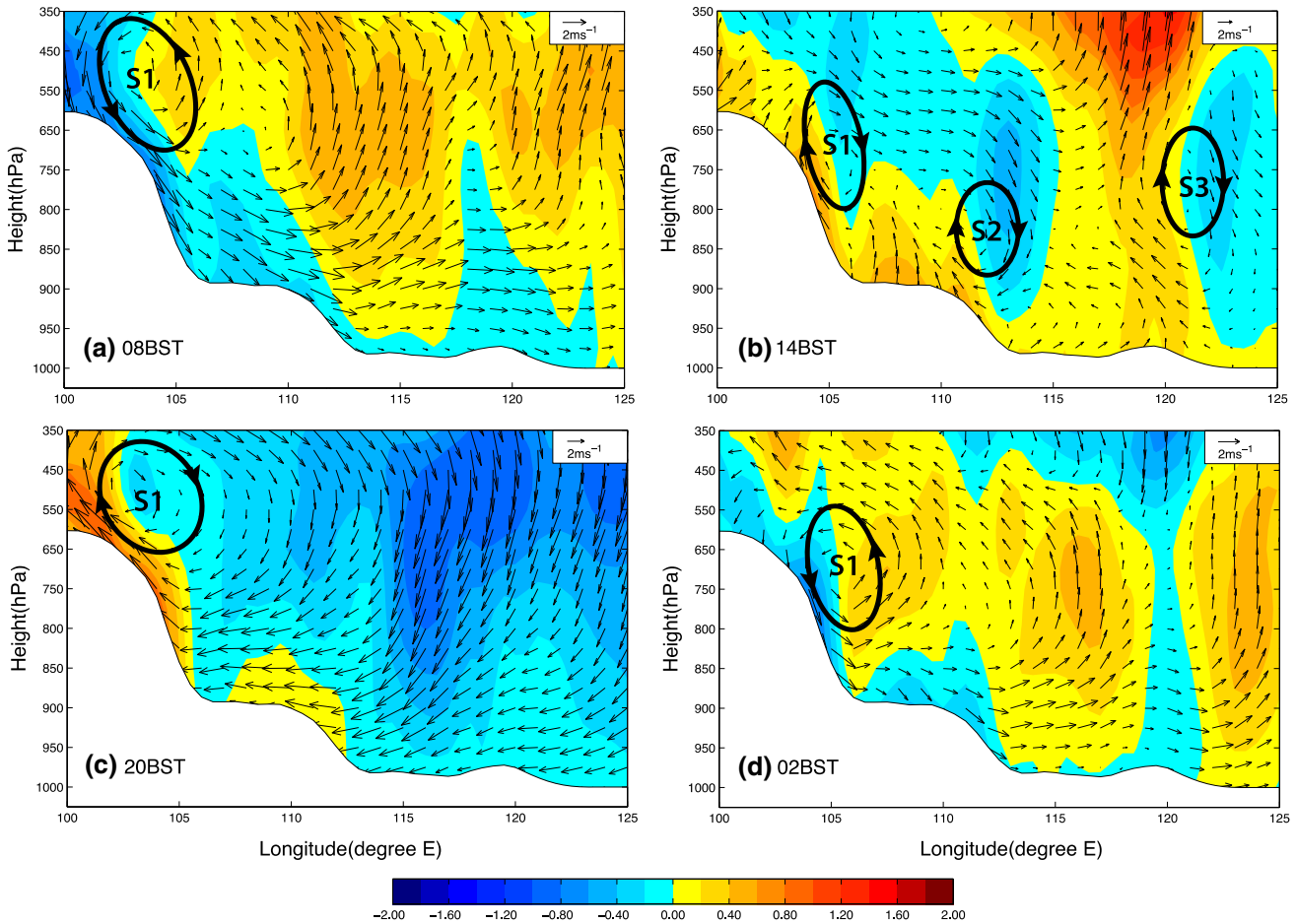

Fig. 9 The same as Fig. 8 but for the TMY period

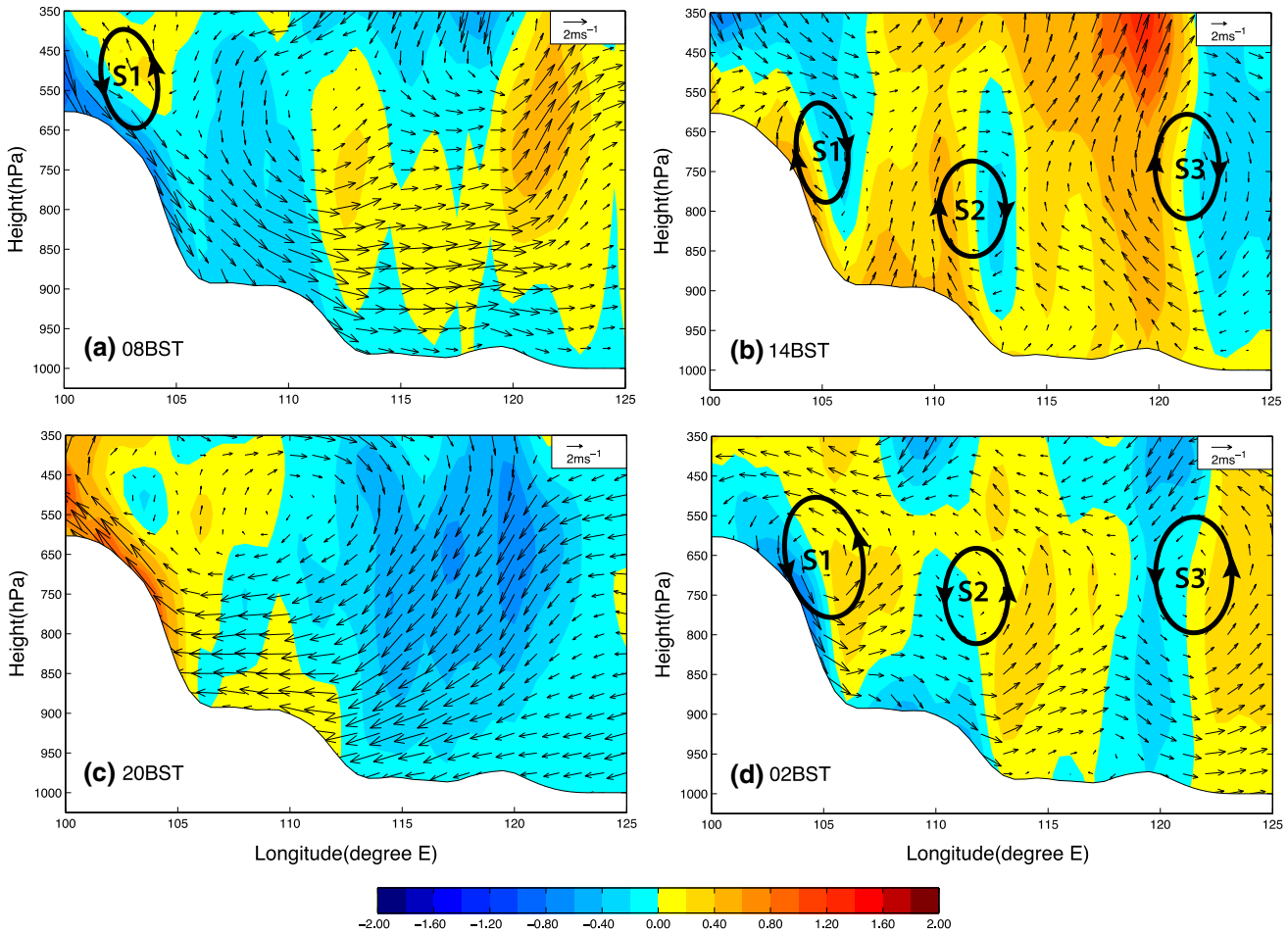

Fig. 10 The same as Fig. 8, but for the post-TMY period

2000 BST with upward motion over the eastern edge of the TP and downward motion over its downstream (Figs. 8c, 9c, 10c), consistent with the strong precipitation over the eastern edge of the TP (Fig. 2b–d). In the late night (0200 BST, Figs. 8d, 10d), due to the heating difference in the evening being opposite to that during daytime, anticlockwise MPS circulations form with upward motion over the SCB, east plains and oceanic areas, and downward motion over the eastern edge of the TP, eastern edge of the "second step" terrain, and the eastern coastline. However, during TMY, there is stronger vertical motion relative to the higher nocturnal rainfall east of the second step terrain. It is found that, because of the nocturnal upward motion and the strong southwesterly wind transporting abundant water vapor, precipitation begins to further increase in the late night (after 0200 BST) east of the "second step" terrain (Fig. 6d) and maximizes after 0800 BST. At 0800 BST, there is one main circulation, with the upward branch at east of the TP and the downward branch over the eastern edge of the TP in the early morning (Figs. 8a, 9a, 10a). But the upward and downward branches of MPS at nighttime (0200 BST) during post-TMY are weaker than those during the former two sub-periods.

The above comparison shows that diurnal variations of MPS circulations and the wind anomaly at low levels are varied during the three sub-periods of the CMYP. During the TMY period, a stronger southwesterly wind and convergence belt during 0200–0800 BST over the Meiyu rain belt enhance the upward motion east of the second step terrain. The upward branch of S2, along with the attendant nocturnal southwesterly wind at lower levels, is primarily responsible for the enhancement along the Meiyu rain belt. Except similarities of daytime MPS circulations (Figs. 8b, 9b, 10b), the thermodynamics MPS circulations during TMY are much stronger than other two sub-periods at nighttime. Additionally, the diurnal variations of precipitation over the TP and SCB are mainly consistent with the effect of heating (MPS circulations) over different distributions of terrain, but over the YHRV it is controlled by background circulation (Meiyu front), diurnal variations of the wind field, and MPS circulations.

5 Conclusion

This study statistically explores the diurnal variations of precipitation of three sub-periods during the Meiyu season from 2003 to 2010 and the impacts of MPS circulations and background circulation on the diurnal variations by dividing the CMYP into the pre-TMY, TMY and post-TMY periods according to observed precipitation days during the CMYP (15 June–15 July, Table 2). The CMORPH precipitation dataset, FNL and CFSR datasets were used to document the diurnal characteristics and eastward propagation of precipitation during the three sub-periods of the CMYP. The major findings of the study can be summarized as follows.

A comparison of the eastward propagation and diurnal variations of precipitation during the three sub-periods showed that the diurnal variations of precipitation over the eastern edge of the TP and SCB are almost consistent with each other, except in terms of their speed of movement and intensity. The precipitation continues to propagate eastward from the east of the "second step" terrain to the central YHRV during the pre-TMY and TMY periods (Table 2), but the phase speed during the pre-TMY is faster. Furthermore, the precipitation can continue to propagate eastward over the YHRV (117°–122°E) during the TMY period. However, precipitation east of the "second step" terrain mainly peaks in the afternoon during the post-TMY period. The average daily precipitation during the TMY period is lower than that during the post-TMY period over the SCB, but east of the SCB it is highest.

A comparison of the diurnal cycles of the horizontal wind anomaly and MPS circulations during the three sub-periods illustrated that the diurnal variations east of the SCB during the TMY period are more obvious than those of the other two sub-periods. The convergence belt over the Meiyu rain belt, combined with the upward branch of MPS circulation, enhances the nighttime precipitation in the western part of the Meiyu rain belt. MPS circulations due to the diabatic heating difference between different terrain distributions are mainly responsible for forcing the diurnal cycles of precipitation over the TP and SCB. As for the diurnal variations of precipitation over the YHRV, diurnal variations of MPS circulations, coupled with the favorable synoptic patterns (Meiyu front), could intensify the precipitation and its diurnal cycles.

In future work, specific case studies and model simulations will be taken into consideration to quantitatively diagnose the dynamic and thermodynamic mechanisms affecting the diurnal cycles.

Acknowledgements This study was supported by the National Key Basic Research and Development Project of China (No. 2012CB417201) and the National Natural Science Foundation of China (Grant Nos. 41375053 and 41505038).

References

Bao X, Zhang F, Sun J (2011) Diurnal variations of warm-season precipitation east of the Tibetan Plateau over China. Mon Weather Rev 139(9):2790–2810

Blackadar AK (1957) Boundary layer wind maxima and their significance for the growth of nocturnal inversions. Bull Am Meteorol Soc 38:283–290

Bonner WD (1968) Climatology of the low-level jet. Mon Weather Rev 96:833–850

Carbone RE, Tuttle JD (2008) Rainfall occurrence in the United States warm season: the diurnal cycle. J Climate 21:4132–4136

Carbone RE, Tuttle JD, Ahijevych D (2002) Inferences of predictability associated with warm season precipitation episodes. J Atmos Sci 59:2033–2056

Chen Y-L, Li J (1995) Large-scale conditions favorable for the development of heavy rainfall during TAMEX IOP 3. Mon Weather Rev 123:2978–3002

Chen G, Sha W, Iwasaki T (2009a) Diurnal variation of precipitation over southeastern China: spatial distribution and its seasonality. J Geophys Res 114:D13103. doi:10.1029/2008JD011103

Chen G, Sha W, Iwasaki T (2009b) Diurnal variation of precipitation over southeastern China: 2. Impact of the diurnal monsoon variability. J Geophys Res 114:D21105. doi:10.1029/2009JD012181

Chen G, Sha W, Iwasaki T, Ueno K (2012) Diurnal variation of rainfall in the Yangtze River Valley during the spring-summer transition from TRMM measurements. J. Geophys. Res. 117:D06106. doi:10.1029/2011JD017056

Chen G, Sha W, Sawada M, Iwasaki T (2013) Influence of summer monsoon diurnal cycle on moisture transport and precipitation over eastern China. J Geophys Res Atmos 118:3163–3177. doi:10.1002/jgrd.50337

Dai A (2001) Global precipitation and thunderstorm frequencies. Part II: diurnal variations. J Climate 14:1112–1128

Dai A, Giorgi F, Trenberth KE (1999) Observed and model simulated precipitation diurnal cycle over the contiguous United States. J Geophys Res 104:6377–6402

Du Y, Zhang QH, Chen Y-L et al (2014) Numerical simulations of spatial distributions and diurnal variations of low-level jets in china during early summer. J Climate 27:5747–5767

Geng B, Yamada H (2007) Diurnal variations of the Meiyu/Baiu rain belt. SOLA 3:61–64

He H, Zhang F (2010) Diurnal variations of warm-season precipitation over NorthChina. Mon Weather Rev 138:1017–1025

Hirose M, Nakamura K (2005) Spatial and diurnal variation of precipitation systems over Asia observed by the TRMM Precipitation Radar. J Geophys Res 110:D05106. doi:10.1029/2004JD004815

Huang HL, Wang CC, Chen GTJ (2010) The Role of diurnal solenoidal circulation on propagating rainfall episodes near the eastern Tibetan Plateau. Mon Weather Rev 138:2975–2989

Joyce RJ, Janowiak JE, Arkin PA (2004) CMORPH: a method that produces global precipitation estimates from passive microwave and infrared data at high spatial and temporal resolution. J Hydrometeorol 5:487–503

Luo Yali, Qian Weimiao, Zhang Renhe, Zhang Da-Lin (2013) Gridded hourly precipitation analysis from high-density rain gauge network over the Yangtze-Huai Rivers Basin during the 2007 Mei-Yu season and comparison with CMORPH. J Hydrometeorol 14:1243–1258

Riley GT, Landin MG, Bosart Lance F (1987) The diurnal variability of precipitation across the central rockies and adjacent great plains. Mon Weather Rev 115:1161–1172

Shen Y, Xiong A, Wang Y, Xie P (2010) Performance of high-resolution satellite precipitation products over China. J Geophys Res 115:D02114. doi:10.1029/2009JD012097

Sun J, Zhang F (2012) Impacts of mountain-plains solenoid on diurnal variations of rainfalls along the Mei-yu front over the East China plains. Mon Weather Rev 140:379–397

Sun JH, Zhou HG, Zhao SX (2006) An observational study of mesoscale convective systems producing severe heavy rainfall in the Huaihe River Basin during 3–5 July 2003. Chin J Atmos Sci 30(6):1103–1118. doi:10.3878/j.issn.1006-9895.2006.06.05 **(in Chinese)**

Tao SY (1980) Rainstorm in China. Science Press, Beijing **(in Chinese)**

Trier SB, Davis CA, Ahijevych DA (2006) Mechanisms supporting long-lived episodes of propagating nocturnal convection within a 7-day WRF model simulation. J Atmos Sci 63:2437–2461

Trier SB, Davis CA, Ahijevych DA (2010) Environmental controls on the simulated diurnal cycle of warm-season precipitation in the continental United States. J Atmos Sci 67:1066–1090

Wallace JM (1975) Diurnal variations in precipitation and thunderstorm frequency over the conterminous United States. Mon Weather Rev 103:406–419

Wang CC, Chen GTJ, Carbone RE (2004) A climatology of warm-season cloud patterns over east Asia based on GMS infrared brightness temperature observations. Mon Weather Rev 132:1606–1629

Wang CC, Chen GTJ, Carbone RE (2005) Variability of warm-season cloud episodes over east Asia based on GMS infrared brightness temperature observations. Mon Weather Rev 133:1478–1500

Wilks DS (2006) Statistical methods in the atmospheric science, vol 91, second version, pp 27–47

Xu WX, Zipser EJ (2010) Diurnal variations of precipitation, deep convection, and lightning over and east of the eastern Tibetan Plateau. J Climate 24:448–465

Yasunari T, Miwa T (2006) Convective cloud systems over the Tibetan Plateau and their impact on meso-scale disturbances in the Meiyu/Baiu frontal zone. J Meteorol Soc Jpn 84(4):783–803

Yu RC, Zhou TJ, Xiong AY (2007) Diurnal variations of summer precipitation over contiguous China. Geophys Res Lett 34:L01704. doi:10.1029/2006GL028129

Zhang SL, Tao SY, Zhang QY (2002) Large and meso-scale characteristics of intense rainfall in the mid and lower reaches of the Yangtze River. Chin Sci Bull 47(9):779–786

Zhang YC, Zhang F, Sun JH (2014a) Comparison of the diurnal variations of warm-season precipitation for East Asia vs. North America downstream of the Tibetan Plateau vs. the Rocky Mountains. Atmos Chem Phys 14:10741–10759

Zhang YC, Sun JH, Fu SM (2014b) Impacts of diurnal variation of mountain-plain solenoid circulations on precipitation and vortices east of the Tibetan Plateau during the Mei-yu season. Adv Atmos Sci 31(1):139–153

Zhao SX, Tao SY, Sun JH (2004) Study on mechanism of formation and development of heavy rainfalls on Mei-yu front in Yangtze River. China Meteorological Press, Beijing **(in Chinese)**